

Structural and optical characterization of Zn doped TiO₂ nanoparticles prepared by sol–gel method

Ruby Chauhan · Ashavani Kumar ·
Ram Pal Chaudhary

Received: 26 June 2011 / Accepted: 20 December 2011 / Published online: 4 January 2012
© Springer Science+Business Media, LLC 2011

Abstract Undoped and zinc-doped TiO₂ nanoparticles (Ti_{1-x}Zn_xO₂ where x = 0.00–0.10) were synthesized by a sol–gel method. The synthesized products were characterized by X-ray diffraction (XRD), scanning electron microscope (SEM), transmission electron microscope (TEM) and UV–VIS spectrometer. XRD pattern confirmed the tetragonal structure of synthesized samples. Average grain size was determined from X-ray line broadening using the Debye–Scherrer relation. The crystallite size was varied from 10 to 40 nm as the calcination temperature was increased from 350 to 800 °C. The incorporation of 3–5 mol% Zn²⁺ in place of the Ti⁴⁺ provoked a slight decrease in the size of nanocrystals as compared to undoped TiO₂. The SEM and TEM micrographs revealed the agglomerated spherical-like morphology with a diameter of about 10–30 nm and length of several nanometers, which is in agreement with XRD results. Optical absorption measurements indicated a blue shift in the absorption band edge upon 3–5 mol% zinc doping. Direct allowed band gap of undoped and Zn-doped TiO₂ nanoparticles measured by UV–VIS spectrometer were 2.95 and 3.00 eV at 550 °C, respectively.

Keywords Nanoparticles · Sol–gel method · Optical absorption · X-ray diffraction (XRD) · UV–vis spectrometer · Scanning electron microscope · Transmission electron microscope

1 Introduction

Nanotechnology for materials, as the one of innovative technologies in the twenty-first century, is expected to revolutionize materials and their applications. The structural, electronic and optical properties can be tuned by controlling the sizes of nanoparticles [1, 2]. Nanocrystalline TiO₂ is a well known semiconductor with photocatalytic activities and has a great potential for applications like in environmental purification, decomposition of carbonic acid gas, pigments, catalyst supports, fillers, coatings, photoconductors, solar cells, gas sensors, biomaterials, dielectric materials and generation of hydrogen gas, etc. [3, 4]. It is also stable in different chemical environment, non-toxic and inexpensive. It has three different crystalline phases: rutile, anatase and brookite, among which rutile is in thermodynamically stable state while the latter two phases are in metastable state. Anatase and rutile have a tetragonal unit cell. Rutile phase contains two TiO₂ molecules per unit cell having a = 4.5937 Å and c = 2.9587 Å and anatase contains four TiO₂ molecules per unit cell having lattice constant a = 3.7842 Å and c = 9.5146 Å. TiO₂ has a wide energy band-gap of 3.0–3.2 eV which prevents the utilization of visible-light that accounts for most of solar energy. Photocatalytic activity of titania may strongly depend on its phase structure, crystallite size, the specific surface area and pore structure. Many studies have confirmed that the anatase phase of TiO₂ is the superior photocatalytic material for air purification, water disinfection, hazardous waste remediation, and water purification [5, 6].

R. Chauhan · R. P. Chaudhary
Department of Chemistry, Sant Longowal Institute
of Engineering and Technology, Longowal 148106, India

R. Chauhan
Technology Education and Research Integrated Institutions,
Kurukshetra 136119, India

A. Kumar (✉)
Department of Physics, National Institute of Technology,
Kurukshetra 136119, India
e-mail: ashavani@yahoo.com

Transition metals ion doping has been primarily studied to enhance the photocatalytic activity under UV irradiation. For the preparation of nanocrystalline particles, wet chemical synthesis routes including sol–gel [7–9], hydrothermal [10–15] and precipitation [16] methods are widely used. For the past two decades, the sol–gel routes have become an appropriate method for the preparation of nanocrystalline materials [17, 18]. Synthetic routes of TiO₂ production usually result in amorphous solid TiO₂ or anatase or rutile depending on the preparation route and the experimental conditions. It is also known that the transformation behavior from amorphous to anatase or rutile phase is influenced by the synthesis conditions. During TiO₂ sol–gel synthesis the temperature of calcinations (and pH value) influence on type of phase [19]. Anatase nanoparticles obtained by sol–gel method are amorphous in phase, but with increasing the temperature up to 350 °C or higher the transition from amorphous to anatase phase happens [20]. However, calcinations temperature must be kept lower than 600 °C, because of the phase transition from anatase to rutile phase [21].

In the present study, undoped and Zn-doped TiO₂ nanoparticles were synthesized by sol–gel method using stabilizing agent like citric acid and polyethylene glycol (PEG) as a capping agent. Polymer capping of the synthesized TiO₂ particles showed an improved stability against agglomeration and photo-degradation.

2 Experimental

2.1 Chemicals

For the preparation of undoped and zinc-doped TiO₂ nanoparticles, the materials used were polyethylene glycol [M = 6,000, OH(OCH₂CH₂)_nH; PEG], titanium tetra-isopropoxide [M = 284, Ti(OC₃H₇)₄], zinc nitrate [M = 297, Zn(NO₃)₂·6H₂O], citric acid [M = 210.14, C₆H₈O₇·H₂O]. All chemicals were AR grade from Sigma Aldrich and used without further purification.

2.2 Synthesis

For the preparation of TiO₂ nanoparticles Ti(IV)-isopropoxide is used as a starting product. TiO₂ sol was prepared by mixing 0.1 M titanium tetra-isopropoxide [Ti(OC₃H₇)₄] and 100 ml of distilled water at room temperature. After stirred the solution for 30 min, 0.05 M citric acid were added into the solution and then capping agent 0.5 gm polyethylene glycol (PEG) was added to prevent agglomeration of particles.

The solution was successively stirred till a clear and transparent acid sol (pH = 3.06 ± 0.15) was obtained. The

TiO₂ sol was dried at 100 °C in the oven for 72 h to get TiO₂ gel. Then the gel was calcined at 350, 550 and 800 °C to prepare TiO₂ powders for about 35–80 min with a heating rate of about 10 °C per minute in a muffle furnace. The Zn-doped TiO₂ sol and powders were prepared by the same procedure as stated above. The only difference was the addition of 0.1 M zinc nitrate [Zn(NO₃)₂·6H₂O] solution into the TiO₂ sol with citric acid as a stabilizer. The zinc concentration was varied to 3, 5 and 10 mol%. The pH of the sol was measured even after addition of zinc nitrate at various concentrations and found to be 3.18 ± 0.15.

2.3 Characterization

X-ray diffraction (XRD) patterns were recorded on a Rigaku mini desktop diffractometer using graphite filtered CuK_α radiation ($\lambda = 1.54 \text{ \AA}$) at 40 kV and 100 mA with a scanning rate of 3 degree per minute (from $2\theta = 20^\circ$ to 80°). The phase content of a sample can be calculated from the integrated intensities of anatase (101), rutile (110) and brookite (121) peaks. If a sample contains only anatase and rutile, the mass fraction of rutile (W_R) can be calculated from the relation [22].

$$W_R = \frac{A_R}{0.886A_A + A_R}$$

where A_A and A_R represent the integrated intensity of the anatase (101) and rutile (110) peaks, respectively.

Optical absorption spectra were recorded on a shimadzu double beam double monochromator spectrometer (UV-2,550), equipped with an integrated sphere assembly ISR-240A in the range of 190–900 nm.

Morphology and sizes of the product were determined by scanning electron microscope (SEM: ZEISS EVO MA-10) equipped with an energy dispersive spectrometer (EDS: Oxford Link ISIS 300) and TEM carried out using a H-7,500 model (Hitachi Ltd., Tokyo, Japan). Diluted nanoparticles suspended in absolute ethanol were introduced on a carbon coated copper grid, and were allowed to dry in air for conducting TEM studies.

3 Results and discussion

3.1 X-ray diffraction studies

Figure 1 a, b, c show the XRD diffraction patterns of undoped and zinc-doped titanium dioxide (Ti_{1-x}Zn_xO₂, where x = 0.00, 0.03, 0.05, 0.10) powder samples calcined at 350, 550 and 800 °C, respectively indicating that all the samples were composed of mainly anatase and partially rutile phase. Peaks marked (A) and (R) correspond to anatase and rutile phases, respectively. The sample prepared at 100 °C was largely

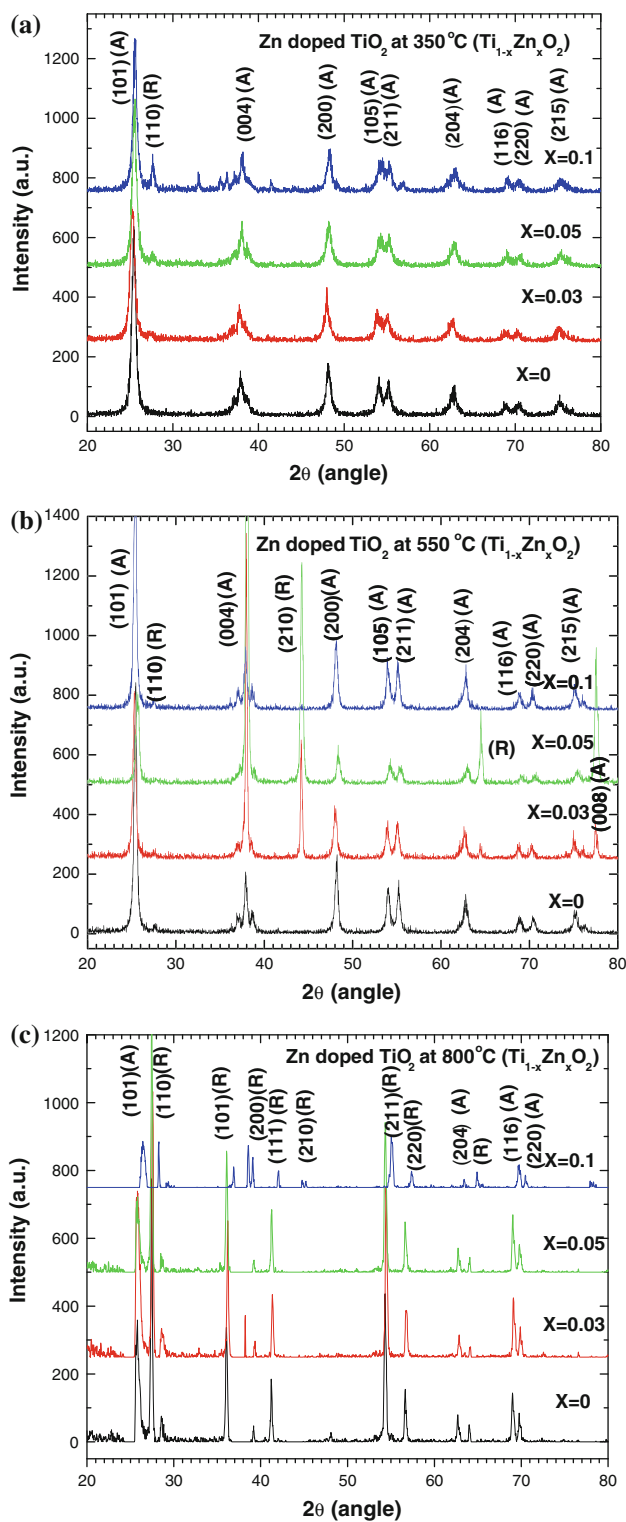


Fig. 1 XRD patterns of undoped and Zn-doped TiO₂ nanoparticles calcined at **a** 350 °C **b** 550 °C and **c** 800 °C with PEG

amorphous. Calcination is a common treatment used to improve the crystallinity of TiO₂ powders. When TiO₂ powder was calcined at 350–800 °C the transformations such as

amorphous to anatase and rutile phase occur. The XRD pattern of annealed samples at 350, 550 and 800 °C exhibits anatase peaks at angles (2θ) = 25.3°, 37.9°, 48.0°, 53.8°, 55°, 62.7°, 68.8°, 70.0°, 75.0° correspond to the reflections from (101), (004), (200), (105), (211), (204), (116), (220), (215) crystal planes of the tetragonal titanium dioxide structure but at 800 °C, large traces of rutile phase are formed. The characteristics peaks of rutile phase at 800 °C are at angles (2θ) = 27.4°, 36.0°, 39.2°, 41.2°, 44.0°, 54.3°, 56.6°, 64.0° correspond to the reflections from (110), (101), (200), (111), (210), (211), (220) crystal planes. All the diffraction peaks agreed with the reported JCPDS card no. 84–1,286 for anatase and 78–2,485 for rutile. No additional peaks corresponding to the secondary phases of zinc oxides were obtained for x = 0.03–0.10 at 350, 550 and 800 °C. It was clearly observed from the XRD patterns that with the increase in temperature of calcinations at 300–800 °C, the diffraction peaks become sharper and stronger; which suggests that the crystalline quality of the nanoparticles are improved and the particle size is increased. Observations from XRD pattern show that the relative intensities of anatase and rutile diffraction peaks are different for the TiO₂ powders obtained at 350, 550 and 800 °C. The results are depicted in Table 1. It can also be seen that the mass fraction of rutile phase slightly increases with increasing calcination temperature. At 800 °C, the mass fraction of rutile was increased up to 51%. Therefore, it is reasonable to suggest that a large amount of anatase phase was transformed into rutile phase.

Usually, the temperature of phase transformation from anatase to rutile depends upon the particle size, morphologies of crystals and additives [23]. The lattice parameters *a* and *c* for the tetragonal structure can be calculated by the following equation [24]:

$$\frac{1}{(d_{hkl})^2} = \frac{h^2 + k^2}{a^2} + \frac{l^2}{c^2}$$

where *h*, *k* and *l* are the Miller indices of the peak, and *d* is the planar distance. From the values of *a* and *c*, the unit cell volume can be determined.

The calculated lattice parameters for anatase TiO₂ are *a* = 3.76 Å, *c* = 9.57 Å and anatase Ti_{0.97}Zn_{0.03}O₂ are *a* = 3.78 Å, *c* = 9.65 Å, respectively. The lattice parameters of Ti_{0.97}Zn_{0.03}O₂ are found slightly increased due to the smaller ionic radius of Zn²⁺ than that of Ti⁴⁺ (*r*Ti⁴⁺ = 0.68 Å, *r*Zn²⁺ = 0.60 Å), which indicates that the doping of Zn does not change the tetragonal structure of TiO₂.

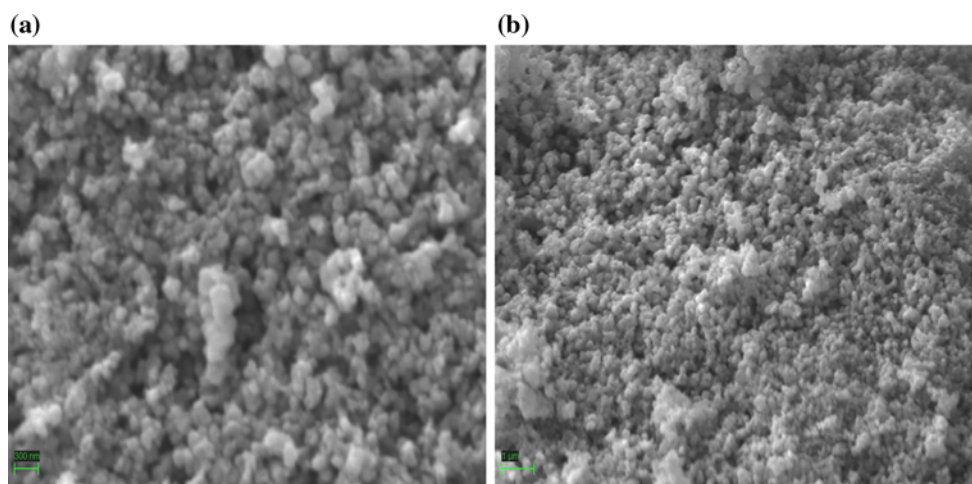
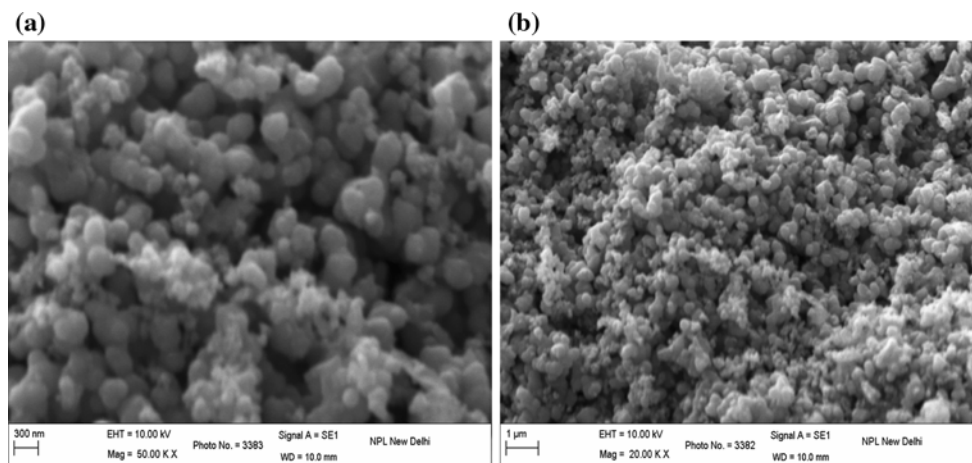
The average crystalline size was calculated from the full-width at half-maximum (FWHM) of XRD lines by using the Debye–Scherrer formula:

$$D_{hkl} = 0.9\lambda / (\beta_{hkl} \cos\theta)$$

where *D* is the average crystallite diameter, *λ* is the wavelength used in angstrom, *β* is the line width at half-maximum

Table 1 Particles sizes calculated by XRD calcined at 350, 550 °C for anatase phase only and the percentage values of rutile and anatase phase content and particle sizes at 800 °C

% of Zn	Calcination temperature (°C)					
	At 350 °C		At 550 °C		At 800 °C	
	Anatase particle size	Anatase particle size	W_A (Fraction of anatase)	W_R (Fraction of rutile)	Anatase particle size	Rutile particle size
0	14	24	48.5	51.5	32	39
3	13	20	48.5	51.5	31	38
5	13	23	55.1	44.9	32	39
10	15	25	77.1	22.9	33	39

**Fig. 2** SEM images of undoped TiO₂ nanoparticles calcined at 350 °C with PEG at different magnification**Fig. 3** SEM images of 5 mol% Zn-doped TiO₂ nanoparticles calcined at 350 °C with PEG at different magnification

and θ is the Bragg angle. The average crystallite size of anatase and rutile TiO₂ nanoparticles were determined from the broadening of the anatase (101) peak at ($2\theta = 25.3$) and rutile (110) peak at ($2\theta = 27.4$). The results are given in Table 1. It can be seen that the average size of nanoparticles increases as

the calcinations temperature is increased and decreases as the percentage doping of zinc is increased from 3–5 mol%. This is due to the change of growth rate between the different crystallographic planes. The calculated values of particles size are presented in Table 1 for undoped and Zn doped (3–10 mol%)

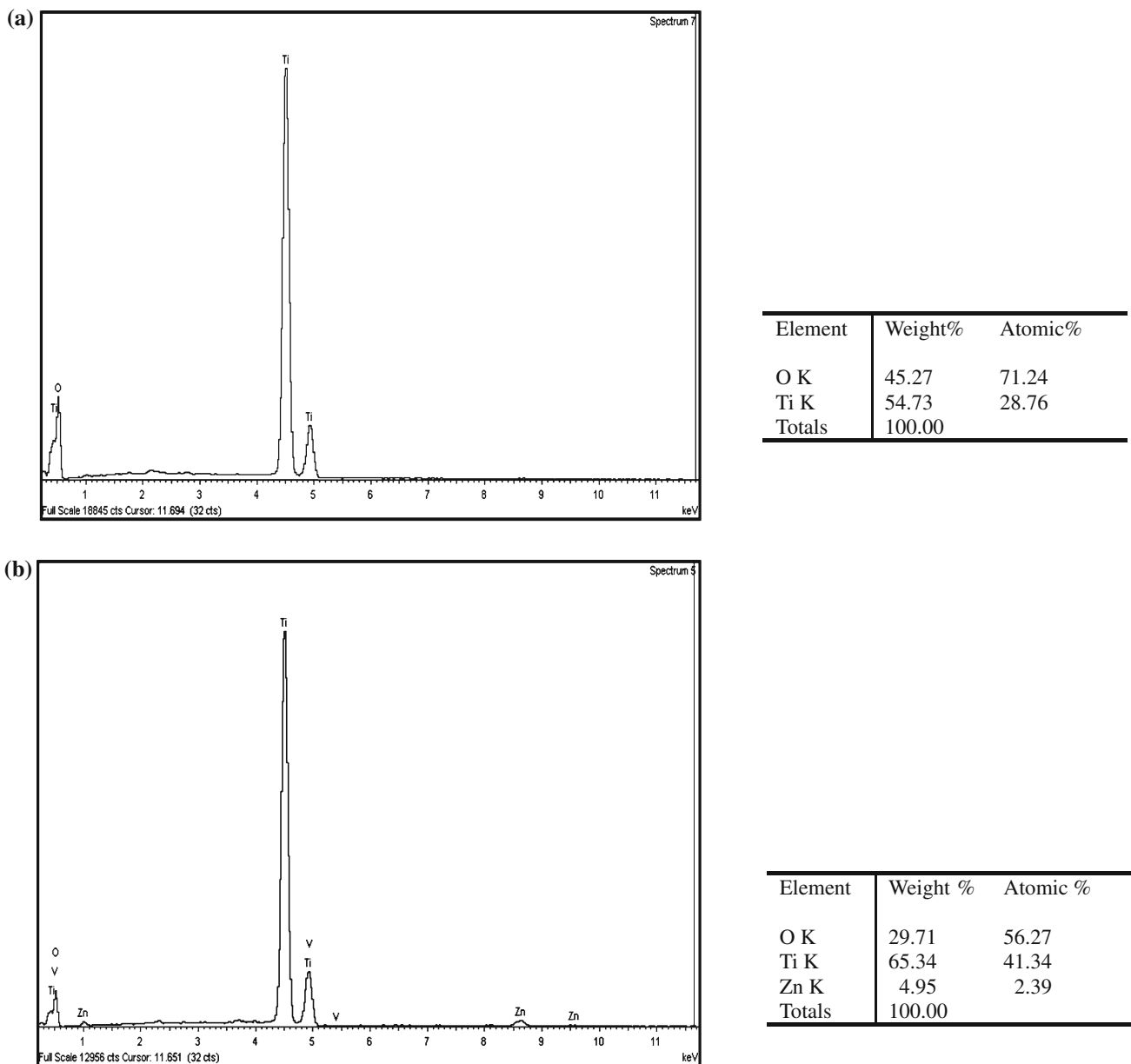


Fig. 4 Energy dispersive X-ray analyses of **a** undoped and **b** 5 mol% Zn-doped TiO_2 nanoparticles calcined at 350°C with PEG

TiO_2 calcined at 350 , 550 and 800°C . The particles size of anatase phase is in the range of 13 – 15 nm, 20 – 25 nm and 31 – 33 nm at 350 , 550 and at 800°C corresponding to the $\text{Ti}_{1-x}\text{Zn}_x\text{O}_2$ ($x = 0.0$ – 0.10) nanoparticles, respectively.

3.2 SEM and TEM studies

Figure 2a, b show the SEM images of undoped TiO_2 and Fig. 3a, b show the SEM images of 5 mol% Zn doped TiO_2 . The elemental analysis were also performed with Energy dispersive X-ray analyses (EDAX) as shown in Fig. 4a, b undoped 5 mol% Zn doped TiO_2 nanoparticles. It is clear from the elemental analysis that 4.95% Zn

element is present in the doped samples and it can also be revealed from the analysis that the Zn^{2+} ions are incorporated in Ti^{4+} lattice sites.

Figure 5a, b show TEM images of undoped and 5 mol% Zn doped TiO_2 at 350°C and observed that the particle morphology is spherical in general. The spheres consist of many small spherical crystals of TiO_2 due to agglomeration. It can be seen that the particle size of pure TiO_2 is about 10 – 20 nm in near agreement with the sizes estimated from XRD (ca. 14 nm). 5 mol% Zn^{2+} doping in the sol–gel method has little influence on the particle size of TiO_2 . From SEM micrograph, non-uniform distribution of particles is found. They consist of either some single particle or cluster of particles.

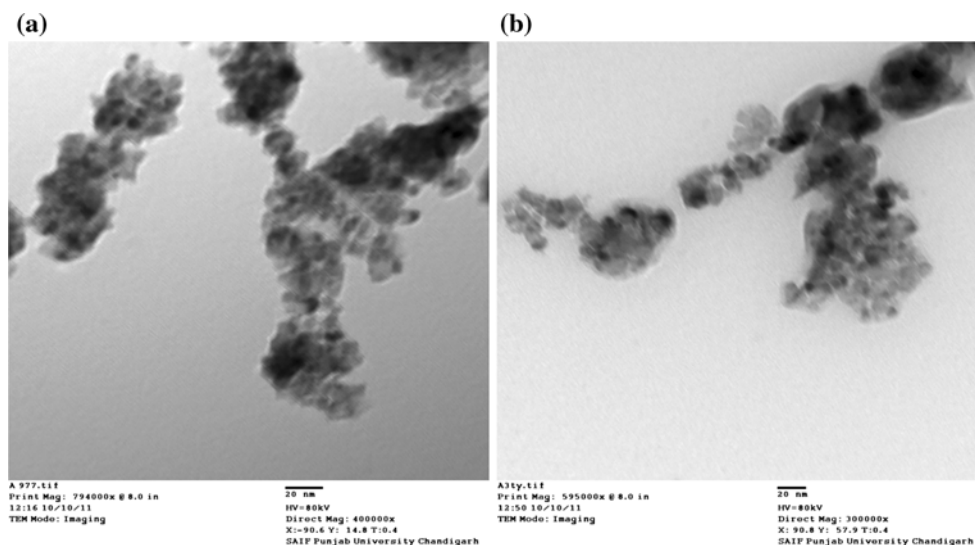


Fig. 5 TEM images of **a** undoped and **b** 5 mol% Zn-doped TiO₂ nanoparticles calcined at 350 °C with PEG

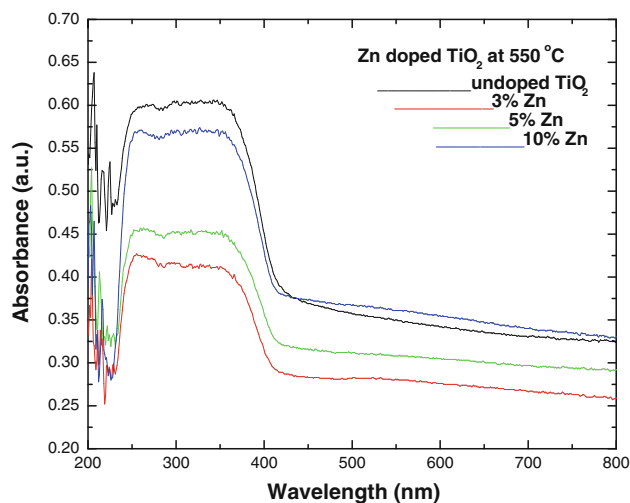


Fig. 6 Optical absorption spectra of undoped and 3, 5, 10 mol% Zn-doped TiO₂ nanoparticles calcined at 550 °C

3.3 Optical studies

The optical absorption spectra of undoped and Zn-doped titanium dioxide (Ti_{1-x}Zn_xO₂ where, $x = 0.00, 0.03, 0.05, 0.10$) samples calcined at 550 °C, and recorded by a UV–VIS spectrometer in the range of 200–800 nm are presented in Fig. 6. The absorption edge shifted towards the shorter wavelength side in 3–5 mol% Zn-doped TiO₂ nanoparticles. Manifacier model is used to determine the absorption coefficient from the absorbance data [25]. The fundamental absorption, which corresponds to the transmission from valance band to conduction band, is employed to determine the band gap of the material. The direct band gap energy can be estimated from a plot of

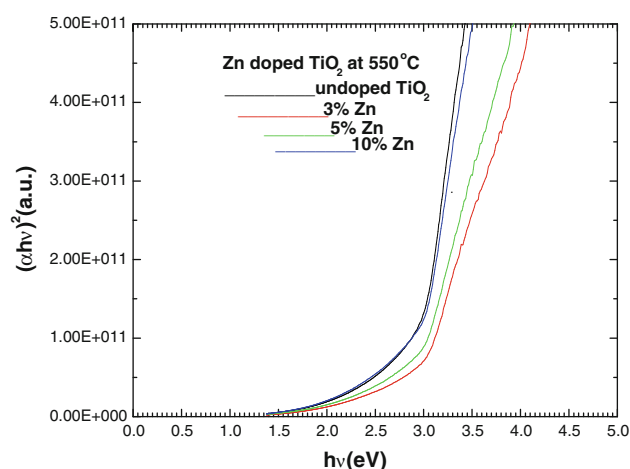


Fig. 7 $(\alpha hv)^2$ versus photon energy ($h\nu$) for undoped and 3, 5, 10 mol% Zn-doped TiO₂ nanoparticles calcined at 550 °C

$(\alpha hv)^2$ versus photo energy ($h\nu$). The energy band gap is determined by using the relationship:

$$\alpha hv = A(h\nu - E_g)^n$$

where $h\nu$ = photon energy, α = absorption coefficient ($\alpha = 4\pi k/\lambda$; k is the absorption index or absorbance, λ is the wavelength in nm), E_g = energy band gap, A = constant, $n = 1/2$ for the allowed direct band gap. The exponent n depends on the type of transition and it may have values 1/2, 2, 3/2 and 3 corresponding to the allowed direct, allowed indirect, forbidden direct and forbidden indirect transitions, respectively [26]. The value of band gap was determined by extrapolating the straight line portion of $(\alpha hv)^2 = 0$ axis; as shown in Fig. 7 at a temperature of 550 °C. The plots of $(\alpha hv)^2$ versus $h\nu$ are

Table 2 Variations of the band gap with temperature of undoped and Zn-doped TiO₂ nanoparticles

% of Zn	Band gap (eV) at 550 °C
0	2.95
3	3.00
5	3.00
10%	2.95

presented in Fig. 7. The intercept of the tangent to the plot will give a good approximation of the direct band gap energies of the samples. The band gap energies of undoped and Zn-doped TiO₂ powders calcined at 550 °C were shown in Table 2. The band gap increases from 2.95 to 3.00 eV with zinc doping (3–5 mol%) at temperature 550 °C. The samples are the combination of anatase and rutile phase and obtained values for E_g are in accordance with values from the literature for pure anatase and rutile phase.

4 Conclusion

Undoped and Zn-doped TiO₂ nanoparticles (Ti_{1-x}Zn_xO₂ where x = 0.00–0.10) were successfully synthesized using sol–gel method. The synthesized particles are in the nanometer regime and the size of anatase crystals were found to be 13–33 nm as estimated from Debye–Scherrer formula. For the sample prepared at 350 °C, the mass fraction of rutile was zero but at 800 °C, the mass fraction of rutile was reached up to 51%. Therefore, it is reasonable to suggest that a large amount of anatase phase was transformed into rutile phase at higher temperature. SEM images revealed that the particles form a cluster of nanocrystalline TiO₂ due to agglomeration. The porosity may result from the evaporation of the aqueous polyethylene glycol when calcined at high temperatures. The optical measurements yield energy band gaps. The absorption edge shifted towards the shorter wavelength side in 3–5 mol% Zn-doped TiO₂ nanoparticles. The band gap value of as prepared Zn doped TiO₂ samples were found to increase as compared to undoped TiO₂. The TiO₂ capped with PEG restricted the agglomeration of the particles.

Acknowledgments Authors are thankful to Dr. Sanjeev Aggrawal and Nidhi Sekhawat, Kurukshetra University, Kurukshetra for

technical support for getting UV–VIS spectra and National Physical Laboratory, New Delhi for getting SEM images. We are thankful to the Director, NIT, Kurukshetra for XRD and SEM facilities in physics department. Authors are also thankful to the reviewers of the manuscript, as the same have been improved only after their valuable suggestions and comments.

References

- Cahn RW (1990) *Nature* 348:389
- Gleiter H (1995) *Nanostruct Mater* 6:3
- Mills A, Elliott N, Hill G, Fallis D, Durrant JR, Willis RL (2003) *Photochem Photobiol Sci* 2:591
- Zhao L, Yu Y, Song L, Hu X, Larbot A (2005) *Appl Surf Sci* 239:285
- Hoffmann MR, Martin ST, Choi W, Bahnemann DW (1995) *Chem Rev* 95:69
- Fujishima A, Rao TN, Tryk DA (2000) *J Photochem Photobiol C* 1:1
- Geuzens E, Vanhoyland G, D'Haen J, Van Bael MK, Van den Rul H, Mullens J, Van Poucke LC (2004) *Key Eng Mater* 264–268:343
- Wang C–C, Ying JY (1999) *Chem Mater* 11:3113
- Li B, Wang X, Yan M, Li L (2002) *Mater Chem Phys* 78:184
- Yang J, Mei S, Ferreira JMF (2004) *J Eur Ceram Soc* 24:335
- So WW, Park SB, Kim KJ, Moon SJ (1997) *J Colloid Interface Sci* 191:398
- Su C, Tseng CM, Chen LF, You BH, Hsu BC, Chen SS (2006) *Thin Solid Films* 498:259
- Yang J, Mei S, Ferreira JMF (2001) *J Am Ceram Soc* 84:1696
- Cheng H, Ma J, Zhao Z, Qi L (1995) *Chem Mater* 7:663
- Reddy KM, Guin D, Manorama SV, Reddy AR (2004) *J Mater Res* 19:2567
- Li ZJ, Hou B, Xu Y, Wu D, Sun YH (2005) *Acta physicochim sin* 21:229
- Gopal M, Moberly Chan WJ, De Jonghe LC (1997) *J Mater Sci* 32:6001
- Kumer KNP, Keizer K, Burggraaf AJ, Okubo T, Nagamoto H, Morooka S (1992) *Nature* 358:48
- Golubovic A, Scepanovic M, Kremenovic A, Askrabic S, Berc V, Dohcevic-Mitrovic Z, Popovic ZV (2009) *J Sol–Gel Sci Technol* 49:311
- Liu AR, Wang SM, Zhao YR, Zheng Z (2006) *Mater Chem Phys* 99:131
- Sugimoto T, Zhou X, Muramatsu A (2003) *J Colloid Interface Sci* 259:43
- Zhang H, Banfield JF (2000) *J Phys Chem B* 104:3481
- Wu M, Lin G, Chen D, Wang G, He D, Feng S, Xu R (2002) *Chem Mater* 14:1974
- Cullity BD, Stock SR (2001) *Elements of X-ray diffraction*, 3rd edn. Prentice-Hall, Inc., Upper Saddle River, NJ, p 619
- Manificier JC, De Murcia M, Fillard JP, Vicario E (1997) *Thin Solid Films* 41:127
- Pankove JI (1971) *Optical process in semiconductors*, Inc. Prentice-Hall, Englewood Cliffs, NJ